AD-A081 643 COMMUNICATIONS RESEARCH CENTRE OTTAWA (ONTARIO) F/G 17/9
A UNIFIED FORMULATION OF SYNTHETIC-APERTURE RADAR THEORY,(U)
DEC 79 E B FELSTEAD
UNCLASSIFIED CRC-1331 NL

1 OF 1
AD A081643

END
DATE FILMED
4-80
DTIC

Communications Research Centre

A UNIFIED FORMULATION OF SYNTHETIC-APERTURE RADAR THEORY

by

E.B. Felstead

This work was sponsored by the Department of National Defence, Research and Development Branch, under Project No. 33C74.

DEPARTMENT OF COMMUNICATIONS
MINISTÈRE DES COMMUNICATIONS

CRC REPORT NO. 1331

CANADA

OTTAWA, DECEMBER 1979

COMMUNICATIONS RESEARCH CENTRE

DEPARTMENT OF COMMUNICATIONS
CANADA

(6)

A UNIFIED FORMULATION OF SYNTHETIC-APERTURE RADAR THEORY

by

(10) E.B. Felstead

(Radio and Radar Research Branch)

(14) CRC [redacted] 1331

(11) December 1979
OTTAWA

(12) 45

This work was sponsored by the Department of National Defence, Research and Development Branch, under Project No. 33C74.

404957

TABLE OF CONTENTS

A UNIFIED FORMULATION OF SYNTHETIC-APERTURE RADAR THEORY

by

E.B. Felstead

ABSTRACT

A theory of synthetic-aperture radar (SAR) is formulated for the case where the radar antenna is pointed along or close to the normal to the track of the satellite or aircraft carrying the radar. All the common signal defects are presented and incorporated into a unified mathematical description of the recorded input signal. From this description, the two-dimensional Fourier transform and the output image function are derived. Signal defects arising from range curvature, rotation of the earth, earth curvature, and antenna pointing error are included in the formulation. A method of correcting for the effects of range curvature by use of a frequency-plane filter is recommended. The direct effects of cross-track motion caused by the earth's rotation are eliminated by proper choice of the coordinate system. Simple methods of handling other aberrations are presented. Further topics covered are ambiguities, the spread of range and latitude over which a single reference function may be used, incoherent integration for reduction of radar speckle, object motion, and antenna motion errors.

1. INTRODUCTION

Synthetic-aperture radar (SAR) has been extensively studied [1]-[4] and much excellent imagery produced. Under certain conditions the return signal contains aberrations that cause problems in the production of high quality imagery. These conditions arise especially on satellite-borne SAR. There has been a tendency to consider each problem individually, in isolation

from other factors. Although such an approach is handy for quick approximations, it can lead to inaccuracies and misinterpretations. In this paper all the common signal defects are presented and incorporated into a unified mathematical description of the recorded input signal. From this input signal, the Fourier transform and the image plane function are derived. These three functions form the mathematical basis for devising signal processing concepts.

Although the discussion in this paper concentrates on satellite-borne SAR, the results can be easily simplified to apply to airborne SAR. The formulation is presented in a form appropriate for optical processing. However, it would be relatively simple to reformulate into a form appropriate for digital processing. Also, the theory deals only with the SAR antenna pointing normal or near normal to the direction of travel (sidelooking). A theory for antennas pointed at large angles from the normal (squinted) has been developed elsewhere [5].

There are four aberrations of the received signal considered here. The first [6], sometimes called "range curvature" [7], arises from the fact that the distance between the SAR and a point object varies quadratically with time. A second class of aberrations arises from motion of the object or motion errors of the SAR. The earth's rotation [8] is one example of such motion. The third aberration is caused by the combined effect of pitch of the antenna about a horizontal axis and yaw about a vertical axis. These motions point the antenna either ahead of or behind the perpendicular to the flight path. Although pitch and yaw alone do not cause much problem, their effect becomes more serious in the presence of range curvature and motion errors. The fourth aberration arises from the curvature of the flight path and of the earth's surface. Leith [6] has formulated a theory of SAR operation taking range curvature into account. Here, the formulation is extended to include the other aberrations.

In Section 2, a coordinate system is introduced that eliminates problems caused both by the earth's rotation and by curvature of the earth and of the flight path. In Section 3, the form of the received SAR signal is given and the equations describing the recorded signal in its two-dimensional format derived. The three forms of modulation of the recorded signal and their implementations are discussed. The two-dimensional Fourier transform of this signal is derived in Section 4. A discussion on image formation in Section 5 includes a description of the basic correlation process required to produce the image, a description of image characteristics, and a discussion of methods of correction for the aberrations. In Section 6, the problem of ambiguities arising from the pulsed (sampled) nature of the radar is treated. The intervals of range or latitude over which a single reference function adequately matches the signal are specified in Section 7. Incoherent averaging to reduce radar speckle is discussed in Section 8. The effects of both object motion and SAR antenna motion errors are considered in Section 9. Neither the effects of the ionosphere [8],[9] nor the problem of imaging ocean waves [10] are examined here. These problems are as yet unsolved and required further work.

2. SAR GEOMETRY

The instantaneous distance r between the SAR antenna and the object being imaged is important in deriving the equation for the SAR signal. In this section, a coordinate system suitable for satellite-borne SAR is presented. The value of r is then derived in terms of these coordinates.

A spacecraft carries the radar along some orbit such as shown in Figure 1(a). If its altitude h_s is approximately constant for at least a synthetic-aperture length, then the centre of the orbit and the centre of the surface curvature approximately coincide at O. (For non-coincident centres, the following theory needs only minor modifications.) The radius of the earth's surface is r_e and that of the orbit is r_e+h_s. The nadir of the satellite moves along the curved azimuth coordinate x which is fixed to the earth's surface. The satellite has a coordinate position $c_a x$ along the orbit where the constant

$$c_a = (r_e+h_s)/r_e = 1 + h_s/r_e. \tag{1}$$

At some instant of time $t=t_o$ the satellite is at C_o and its nadir is at B_o. Consider a single point reflector on the earth's surface located at A_o, such that the plane $A_oB_oC_o$ is perpendicular to the x coordinate at B_o. The azimuthal position of A_o is the same as that of B_o, i.e., $x=x_o$. The second coordinate of A_o is the slant range r_o, the distance between A_o and C_o. The ground range d_o, the distance along the curved surface between A_o and B_o, is given by $d_o = r_e\theta_r$, where $\theta_r = \angle A_oOC_o$. If the small-angle approximation $\cos\theta_r \simeq 1 - \theta_r^2/2$ is made in

$$r_o^2 = (r_e+h_s)^2 + r_e^2 - 2(r_e+h_s)r_e \cos\theta_r, \tag{2}$$

then the ground range may be expressed in terms of slant range as

$$d_o \simeq c_r \sqrt{r_o^2-h_s^2} \tag{3}$$

which is simply a right-angled triangle relation scaled by a magnification factor

$$c_r = 1/\sqrt{1 + h_s/r_e} = 1/\sqrt{c_a}. \tag{4}$$

The spacecraft's orbital velocity usually is given as the velocity vector $\underline{V}_s$ measured with respect to inertial space. As shown in Figure 2, $\underline{V}_s$ makes an angle ϕ_s to the local meridian. Because of earth rotation, the surface has a velocity vector $\underline{V}_e$ relative to inertial space. The spacecraft's velocity vector $\underline{V}$ along the x axis (see Figure 1(a)) is the velocity relative to the earth's surface. This velocity is calculated from $\underline{V}_s$ and $\underline{V}_e$.

As illustrated in Figure 1(b), the velocity $\underline{V}/c_a$ of the nadir point B_o along the surface is the vector sum of $-\underline{V}_e$ and the velocity $\underline{V}_s/c_a$. Velocity $\underline{V}_e$ has components $\underline{V}_{ep}$ parallel and $\underline{V}_{en}$ normal to the vector $\underline{V}_s/c_a$. From Appendix A, the magnitudes of the components are

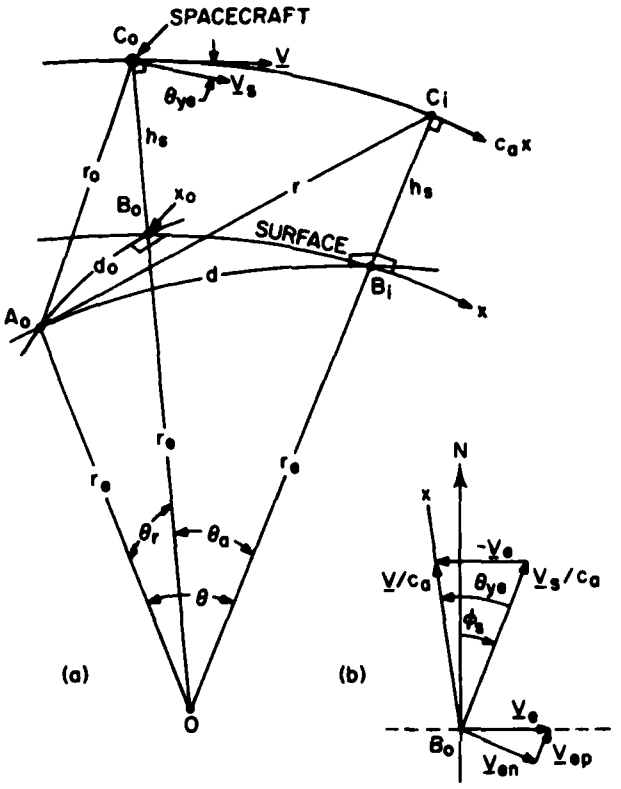

Figure 1. Coordinates, dimensions and velocities used in the formulation of the problem where (a) is a perspective drawing, and (b) shows the plane of the surface at point B_o.

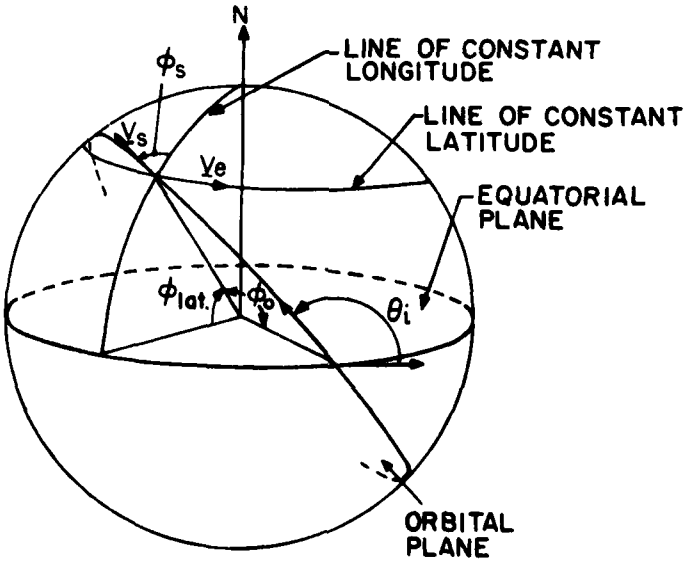

Figure 2. Angles for defining orbit

$$V_{ep} = \omega_e r_e \cos\theta_i \tag{5a}$$

and

$$V_{en} = \omega_e r_e \sin\theta_i \cos\phi_o \tag{5b}$$

where θ_i is the angle of inclination of the orbit, ω_e is the angular velocity of the earth about the N-S axis in radians per unit time, and ϕ_o is the angle of the spacecraft measured from the equator in the orbital plane (see Figure 2). The sign of V_{ep} in (5) is valid for the satellite ascending or descending. The magnitude of $\underline{V}/c_a$ is

$$V/c_a = [V_{en}^2 + (V_{sp}/c_a)^2]^{\frac{1}{2}} \tag{6}$$

and the angle θ_{ye} between $\underline{V}_s/c_a$ and $\underline{V}/c_a$ is

$$\theta_{ye} = \tan^{-1} \frac{V_{en}}{V_{sp}/c_a} \tag{7}$$

where

$$\underline{V}_{sp} = \underline{V}_s - c_a \underline{V}_{ep} \tag{8}$$

is the component of $\underline{V}$ parallel to $\underline{V}_s$. The sign of V_{ep}, as determined by (5b), must be maintained in (8). Since V_{ep} is independent of latitude, and if c_a and V_s are constant, the magnitude of the component $\underline{V}_{sp}$ is constant. The velocity V_{en} of the surface normal to the orbit, is latitude dependent. It is this component of earth rotation that gives rise to certain processing problems. It will be assumed that V_{en} is constant over a single synthetic-aperture length.

The SAR moves along the orbit with velocity $\underline{V}$ to another position C_i at time $t=t_i$. Correspondingly, the nadir moves with a velocity $\underline{V}/c_a$ along the surface to position B_i on the x coordinate. The distance r between the new position C_i of the antenna and the object at A_o on the surface must now be determined. For the triangle A_oOC_i

$$r^2 = r_e^2 + (r_e+h_s)^2 - 2r_e(r_e+h_s)\cos\theta. \tag{9}$$

From the rules of spherical trigonometry for the right spherical triangle $B_oA_oB_i$ shown in Figure 1(a),

$$\cos\theta = \cos\theta_a \cos\theta_r \tag{10}$$

where $\theta = \angle A_oOB_i$ and $\theta_a = \angle C_oOC_i$. If we solve for $\cos\theta_r$ in (2) and note that $\theta_a = (x-x_o)/r_e$ then r becomes

$$r = \left\{ r_e^2 + (r_e+h_s)^2 + [r_o^2 - (r_e+h_s)^2 - r_e^2] \cos \frac{x-x_o}{r_e} \right\}^{\frac{1}{2}}. \tag{11}$$

An expansion in a Taylor series about $x=x_o$ gives

$$r \simeq r_o + \frac{(x-x_o)^2}{2r_o}\left(c_a - \frac{r_o^2-h_s^2}{2r_e^2}\right) . \tag{12}$$

Terms in $(x-x_o)^4$ and higher are, in all practical cases, negligible and are omitted in (12). Usually $c_a >> (r_o^2-h_s^2)/2r_e^2$ so that the term $(r_o^2-h_s^2)/2r_e^2$ may also be omitted. For straight flight over a flat earth, $r_e = \infty$ and $c_a = 1$, so that the expression in (12) reduces to that often given for airborne SAR [1]-[3]. Range r may also be expressed as a function of time since azimuthal distance is related to time by

$$x-x_o = (V/c_a)(t-t_o) . \tag{13}$$

3. FORM OF SAR SIGNAL

As the SAR moves along its orbit, a series of pulses are transmitted. The n^{th} pulse has the form $f(t-n/f_p)\exp(j2\pi f_c t) + c.c.$ where the pulse waveform $f(t) = a(t)\exp[j\alpha(t)]$ is a complex modulation of the coherent carrier wave of frequency f_c, c.c. denotes the complex conjugate of the previous expression, and f_p is the PRF. This signal is coherent from pulse-to-pulse. The signal returned from a point object at A_o is

$$u(t) = \sigma f(t - 2r/c - n/f_p)\exp[j2\pi f_c(t - 2r/c)] + c.c. \tag{14}$$

where c is the velocity of the radar wave and σ is a complex amplitude proportional to the object's reflectivity. Recall that r can be expressed as a function of time. Signal (14) is synchronously demodulated to become

$$u_d(t) = \sigma f(t - 2r/c - n/f_p)\exp(-j4\pi r/\lambda_r)\exp(j2\pi f_o t) + c.c. \tag{15}$$

where f_o is an offset frequency and $\lambda_r = c/f_c$ is the radar wavelength. The demodulation is discussed further in Appendix B.

The signal $u_d(t)$ is a one-dimensional function of time. The purpose of the factor $\exp(j2\pi f_o t)$ will be seen later. The factor $f(t - 2r/c - n/f_p)$ will be seen to lead to an image in the range dimension and the factor $\exp(-j4\pi r/\lambda_r)$ to an image in the azimuth dimension. In order to produce the required two-dimensional image, it is necessary to separate these two factors in some manner. The separation is based on the fact that the range function is very rapidly varying in time compared to the azimuth function. This difference arises because the range signal is associated with the velocity c whereas the azimuth function is associated with the velocity V. To set up the separation, the signal arising from successive transmitted pulses are usually recorded along corresponding successive lines. The range function is recorded along the lines. The azimuth function varies negligibly along one line; its variation appears as a modulation across the lines.

For this discussion it is assumed that the signal is to be recorded on photographic film [1] where the distance x_f along the film represents the azimuth dimension and distance r_f across the film represents the range dimension. For each transmitted pulse a recording beam sweeps out a line across the film at a velocity v_c in the r_f direction. The film is moving at a velocity v_f in the x_f direction. Therefore, distance on the film is related to time by

$$t = x_f/v_f + r_f/v_c. \tag{16}$$

Because of the sampling in azimuth at the PRF, the signal will be recorded only along the lines $x_f/v_f = n/f_p$. Thus, the range function in (15) becomes

$$f(r_f/v_c - 2r/c) = f\left[\frac{2q}{c}(r_f - r/q)\right] \tag{17}$$

where the scaling constant,

$$q = \frac{c}{2v_c} \tag{18}$$

is the range demagnification factor. If the azimuth function is adequately sampled, it is valid, for the purposes of the following discussion, to replace the sampled azimuth variable n/f_p by the continuous variable x_f/v_f. (The effects of sampling are considered later.) Since $x = (V/c_a)t$ and $x_f = v_f t$, range (12) may be written in terms of x_f as

$$r = r_o + \frac{c_a p^2}{2r_o}(x_f - x_o/p)^2 \tag{19}$$

where the scaling constant

$$p = \frac{V/c_a}{v_f} \tag{20}$$

is the azimuth demagnification factor.

The signal in (15) is limited by the region of ground illuminated by the antenna. The region illuminated depends on the antenna beamwidth and pointing direction. In azimuth, let the two-way antenna pattern in amplitude be $h[(x-x_o + x_s)/L]$. It is given here as a function of distance along the ground where x_s is the shift of the beam centre from the perpendicular to track. The effective synthetic-aperture length is

$$L \simeq \beta r_o \tag{21}$$

and β is the effective angular beamwidth, in azimuth, of the two-way amplitude antenna pattern. An angular pointing error θ_s measured in the slant plane from the line C_oA_o may be associated with x_s, where $\theta_s = \tan^{-1}(x_s/r_o)$. In this paper it is assumed that the antenna shift x_s is sufficiently small that,

when inserted into (11), it causes little error in the Taylor series expansion. An angular pointing error θ_s of about 10° to 20° is probably tolerable. For larger pointing errors the antenna is said to be squinted. An expansion about the offset angle θ_s is then necessary for an accurate representation [5].

The shift x_s is composed of several components. First, pitch θ_p, and yaw θ_y, of the antenna causes angular pointing-errors of θ_{ps} and θ_{ys}, respectively, in the slant plane as illustrated in Figure 3. If pitch and yaw are relatively small then

$$\theta_{ps} \simeq \frac{h_s}{r_o}\,\theta_p, \tag{22a}$$

and

$$\theta_{ys} \simeq \frac{\sqrt{r_o^2-h_s^2}}{r_o}\,\theta_y. \tag{22b}$$

The corresponding components of shift x_s are

$$x_{ps} = r_o \tan\theta_{ps} \simeq h_s\theta_p, \tag{23a}$$

and

$$x_{ys}(r_o) = -\,r_o\tan\theta_{ys} \simeq -\sqrt{r_o^2-h_s^2}\;\theta_y. \tag{23b}$$

The signs of θ_p and θ_y in Figure 3 are considered positive. If the antenna were looking to the left, then $x_{ys} = +\,r_o\tan\theta_{ys}$.

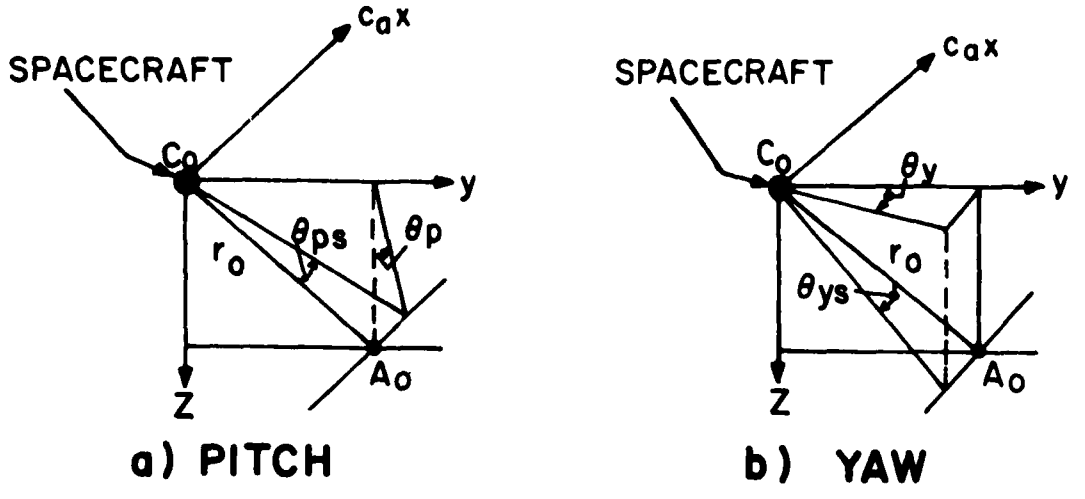

Figure 3. Diagrams defining (a) pitch and (b) yaw angle of the centre of the beam

Another component of x_s arises if the antenna is pointed perpendicular to the inertial-space orbital-velocity vector $\underline{V}_s$ rather than to the velocity vector $\underline{V}$ which is measured relative to the surface. Then the antenna would have an equivalent yaw angle θ_{ye}, which is the angle centred on the satellite between $\underline{V}_s$ and $\underline{V}$ shown in Figure 1(a) and is also the angle centred on B_o between $\underline{V}_s/c_a$ and $\underline{V}/c_a$ shown in Figure 1(b). The θ_{ye} shown in Figure 1(b) is positive. The along-track offset due to the equivalent yaw is

$$x_{yes}(r_o) \simeq r_o \tan\left[-\frac{\sqrt{r_o^2-h_s^2}}{r_o}\,\theta_{ye}\right]. \tag{24}$$

For θ_{ye} small, the substitution of (7) into (24) leads to

$$x_{yes}(r_o) \simeq -\sqrt{r_o^2-h_s^2}\,\frac{V_{en}}{V_{sp}/c_a} = \frac{-\,d_o V_{en}}{c_r V_{sp}/c_a}, \tag{25}$$

which is range and latitude dependent. If the antenna points to the left of track, a left-handed coordinate system may be used. Then the sign of x_{yes} in (24) and (25) is reversed. Note that through the use of a coordinate frame fixed to the surface, the only effect of earth rotation is an equivalent yaw of the antenna resulting in an offset of the antenna pattern. As will be discussed in Subsection 5.4, even this effect may be eliminated by steering the antenna to be perpendicular to $\underline{V}$ (i.e., to point along zero-doppler frequency).

The SAR antenna can have a vertical velocity-component $\underline{V}_v$. If $\underline{V}_v$ is relatively small and slowly varying, its effect is approximately equivalent to that of pitch. Since the antenna velocity is $\underline{V} + \underline{V}_v$ whereas the antenna is nominally perpendicular to $\underline{V}$, the equivalent pitch angle is $\theta_v = \tan^{-1}(V_v/V)$. Thus, the component of x_s caused by vertical velocity is

$$x_{vs} = h_s \tan^{-1}(V_v/V). \tag{26}$$

An exact analysis of the effects of vertical velocity is given in Section 9. The total azimuth shift of the beam centre is

$$x_s(r_o) = x_{ps} + x_{ys}(r_o) + x_{yes}(r_o) + x_{vs}. \tag{27}$$

In the range dimension, the beamwidth and the pointing direction of the antenna limit the width and position of the ground swath illuminated. The effect can be described as a weighting of the signal (15) by the weighting function $h_r(t - 2r_c/c - n/f_p)$, related to the antenna pattern in range, where r_c is the slant range of the beam centre. Antenna roll causes r_c to vary. The effect of roll is to shift the ground swath that can be imaged. Roll has no other effect on the image. For simplicity the weighting function h_r is omitted in the following.

The complete recorded signal is thus,

$$g(x_f,r_f) = \sigma h\left(\frac{x_f - \frac{x_o - x_s(r_o)}{p}}{L/p}\right)$$

$$\times \quad f\left\{\frac{2q}{c}\left[r_f - \frac{r_o}{q} - \frac{c_a p^2}{2qr_o}(x_f - x_o/p)^2\right]\right\}$$

$$\times \quad e^{-j\frac{4\pi}{\lambda_r}\left[r_o + \frac{c_a p^2}{2r_o}(x_f - x_o/p)^2\right]} \quad e^{j2\pi f_o\left(\frac{x_f}{v_f} + \frac{r_f}{v_c}\right)}$$

$$+ \quad \text{c.c.} \qquad (28)$$

The exponential factor containing f_o is a spatial carrier wave. Its purpose is to aid in the separation of the spectrum of the c.c term in (28) from that of the rest of the expression. If f_o is small then, because $v_c >> v_f$, the carrier is approximately $\exp[j2\pi(f_o/v_f)x_f]$, which corresponds to an offset in azimuthal frequency. The spatial-frequency offset in azimuth, $f_{ox} = f_o/v_f$, is selected to be larger than half the bandwidth-in-azimuth of $g(x_f,r_f)$. To obtain a frequency offset in range, the offset f_o must be an exact integer-multiple of the PRF or else a serious error modulation will occur. Thus, if $f_o = Nf_p$, the carrier is $\exp[j2\pi Nn]\exp[j2\pi(f_o/v_c)r_f] = \exp[j2\pi(f_o/v_c)r_f]$, the desired offset-in-range carrier. The spatial-frequency offset in range, $f_{or} = f_o/v_c$, is selected to be larger than half the bandwidth-in-range of $f(x_f,r_f)$. For digital processing it is usually preferred to work at baseband where $f_o = 0$. Then it is necessary to have both an in-phase and a quadrature form of (28) available. An outline of how the three forms are obtained electronically is given in Appendix B. The form of offset does not affect the general theory. Therefore the offset term in (28) will henceforth be omitted. Furthermore, it will be assumed that, with the aid of offsets or in-phase and quadrature processing, the c.c. term can be separated out and it will also be omitted.

In the first exponential factor of (28), the component in x_f^2 is the azimuth-focussing function, and $4\pi r_o/\lambda_r$ is a constant phase. The focussing term is modified by c_a. In the function $f(x_f,r_f)$, the component in x_f^2 is a quadratic displacement in the r_f direction. This displacement is known as range curvature. It is often negligible for low altitude SAR's [1]. The quadratic shape of the envelope of function f is illustrated in Figure 4. The quadratic curve is centred on $(x_o/p,\ r_o/q)$. The range width $R_2/2q$ will be discussed in Subsection 5.2. As indicated by the cross-hatched area of Figure 4, the antenna pattern h and the function f select the section of the complex function that is used.

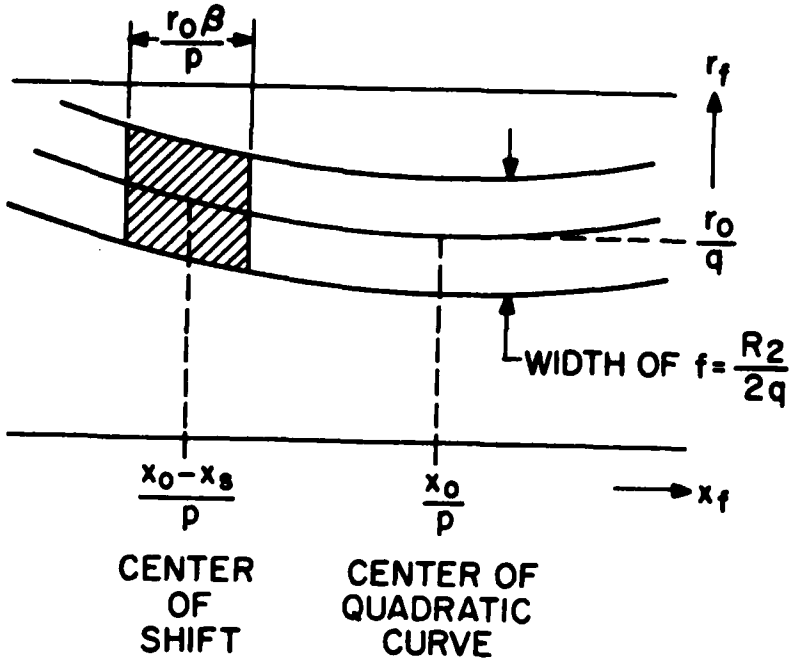

Figure 4. Outline of the envelope of the function $f(x_f r_f)$ limited by $h(x_f)$ as given in (28).

4. THE FOURIER TRANSFORM OF THE INPUT SIGNAL

In many processing methods, frequency plane operations are used. The two-dimensional Fourier transform of $g(x_f,r_f)$ in (28) is shown in Appendix C to be

$$G(f_x,f_r) = c_2\sigma\, F\left(\frac{cf_r}{2q}\right) e^{-j2\pi f_r r_o/q}\, h\left(\frac{f_x - 2c_a p x_s(r_o)/(\lambda_r r_o)}{-2c_a p\beta/\lambda_r}\right) \times e^{\frac{j\pi r_o q f_x^2}{c_a p^2(f_r+2q/\lambda_r)}}\, e^{-j2\pi f_x x_o/p} \tag{29}$$

where f_x is the azimuth spatial frequency and f_r the range spatial frequency, $F(f_r)$ is the Fourier transform of $f(r_f)$, and $c_2 = c[\sqrt{r_o\lambda_r/(2c_a p^2)}/(2q)]$ $\exp(j\pi/4)\exp(-j4\pi r_o/\lambda_r)$, a complex constant. If suitably processed, the $F\exp(-j2\pi f_r r_o/q)$ factors in (29) result in a compressed range signal located at $r_2 = r_o/q$, the desired result, where r_2 is the range dimension in the output plane. The second exponential in (29) contains the desired azimuth focussing function but is aberrated owing to range curvature represented by f_r in the denominator and is scaled by $1/c_a$ because of earth and orbit curvature. The focussing may be separated from the aberration by, first, noting that the maximum value of $(f_r\lambda_r)/(2q)$ is $1/2\ \Delta f/f_c$ where Δf is the bandwidth of $f(t)$ and $f_c = c/\lambda_r$ is the rf carrier frequency. Usually $1/2\ \Delta f/f_c \ll 1$ so that

$$e^{j\frac{\pi\lambda_r r_o f_x^2}{2c_a p^2(1+f_r\lambda_r/2q)}} \simeq e^{j\frac{\pi\lambda_r r_o f_x^2}{2c_a p^2}} e^{-j\frac{\pi\lambda^2 r_o r f_x^2}{4c_a p^2 q}} \tag{30}$$

where the first complex exponential is the desired azimuth focussing-function free of range-curvature effects and the second represents an aberration due to range curvature and is a function of $f_r f_x^2$. If suitable processing is used, the $\exp(-j2\pi f_x x_o/p)$ term results in the azimuth signal being centred on $x_2 = x_o/p$ at the output plane. The form of the azimuth antenna pattern remains h but it is now a function of f_x, and is shifted by the amount $f_x = 2pc_a x_s(r_o)/(\lambda_r r_o)$ because of antenna pointing error. The spatial bandwidth in the f_x dimension of the function h, and therefore of G, is

$$B_{fx} = 2c_a p\beta/\lambda_r = \frac{2V\beta}{\lambda_r}\left(\frac{1}{v_f}\right) \tag{31}$$

and the spatial bandwidth in the f_r dimension is B_{fr}, which is the width of the function $F(cf_r/2q)$.

In converting the demodulated signal of (15) into the recorded signal of (28), the time variable t was separated into two components and converted to the two space variables x_f and r_f according to (16). There is a similar conversion between temporal and spatial frequencies. A temporal frequency ν_r may be associated with the range function f(t) in (15) so that the transform of f(t) is $F(\nu_r)$. The frequency conversion

$$\nu_r = v_c f_r \tag{32}$$

follows from the temporal-to-spatial conversion of (16). Similarly, a temporal frequency ν_x may be associated with the azimuth phase function in (15) so that

$$\nu_x = v_f f_x. \tag{33}$$

It is noted in Appendix C that, for a large time-bandwidth product, there is a one-to-one correspondence between time and frequency for the azimuth phase function. Thus an instantaneous frequency has some physical significance. For the azimuth function in (15), the instantaneous azimuth (doppler) frequency is defined as

$$\nu_{xi} = -(2/\lambda_r)dr/dt. \tag{34}$$

The substitution of (12) and (13) into (34) results in

$$\nu_{xi} = -\frac{2V^2(t-t_o)}{c_a r_o \lambda_r} = -\frac{2V(x-x_o)}{r_o \lambda_r}. \tag{35}$$

The instantaneous spatial frequency in azimuth is found, by differentiating the azimuth focussing function in (28), to be

$$f_{xi} = -\frac{c_a p^2}{\lambda_r r_o}\frac{d(x_f - x_o/p)^2}{dx_f} = \frac{v_{xi}}{v_f} . \tag{36}$$

The temporal azimuth bandwidth B_{vx} is found by letting $x-x_o = L$ in (35) to give

$$B_{vx} = \frac{2V\beta}{\lambda_r} . \tag{37}$$

In the description of the frequency function G, the effects of the azimuth sampling at the PRF f_p, the frequency offsets mentioned in conjunction with (28), and the c.c. term were neglected. If these three factors are included, then the output spectra have the following forms:

Azimuth offset -

$$\sum_{n=-\infty}^{\infty} [G(f_x - f_{ox} - nf_{px}, f_r) + G^*(-f_x - f_{ox} - nf_{px}, -f_r)]$$

Range offset -

$$\sum_{n=-\infty}^{\infty} [G(f_x - nf_{px}, f_r - f_{or}) + G^*(-f_x - nf_{px}, -f_r - f_{or})]$$

Baseband -

I channel

$$\sum_{n=-\infty}^{\infty} [G(f_x - nf_{px}, f_r) + G^*(-f_x - nf_{px}, -f_r)]$$

Q Channel

$$\sum_{n=-\infty}^{\infty} [G(f_x - nf_{px}, f_r) - G^*(-f_x - nf_{px}, -f_r)]$$

where $f_{px} = f_p/v_f$ is the spatial PRF and * denotes complex conjugate. Representations of the envelope hh_r of these spectra are shown in Figure 5. The boundaries obviously will not be as sharp as shown. The same PRF is used in all cases. To avoid overlap of spectra, the PRF must be

$$f_{px} > 2B_{fx} \tag{38a}$$

for azimuth offset but need only be

$$f_{px} > B_{fx} \tag{38b}$$

for range offset and for baseband. Thus, azimuth offset has a disadvantage in requiring a PRF twice as large as that for the other two techniques. The effect of antenna pointing error is to shift the repeated envelope Σh of the repeated spectra ΣG by a distance $2pc_a x_s/\lambda_r r_o$ in the f_x direction. The envelopes of the conjugate spectra ΣG^* are shifted by the same amount but in the opposite direction. These shifts were not included in Figure 5. It is very important to note that the phase functions in ΣG and ΣG^* do *not* shift -

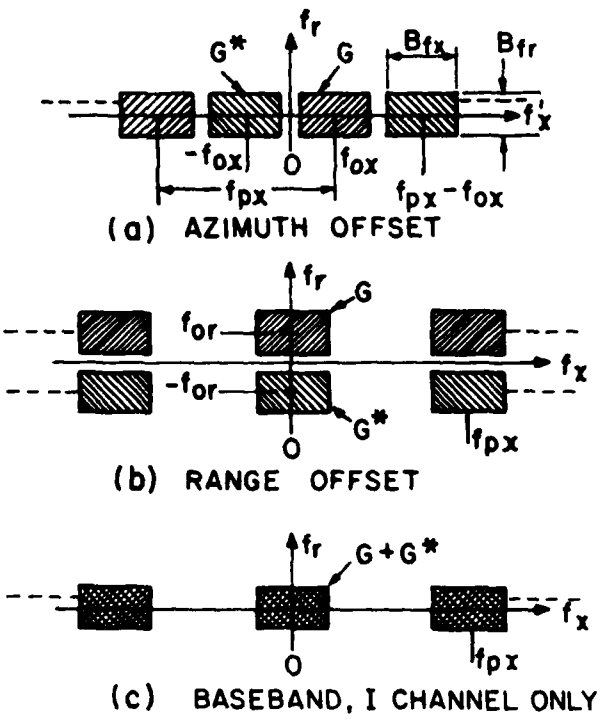

Figure 5. Envelopes of two-dimensional spectra of input signal for 3 forms of frequency offset and all for the same PRF, f_{px}. Right-to-left cross hatching represents the spectrum G and the other represents G (after Harger [3, p. 68]).*

only the envelopes shift. These shifts are discussed further in Subsection 5.2.

In the above, a weighting in the f_x direction over the infinitely repeated spectra has been omitted. The weighting arises because of limited frequency response of the input device.

Sometimes it is useful to do certain operations in a mixed domain, i.e., a domain where space is one dimension and spatial frequency is the other. From Appendix C it can immediately be seen that the one-dimensional transform of $g(x_f,r_f)$ with respect to r_f is

$$G_r(x_f,f_r) = \sigma c_3 F\left[\frac{c}{2q} f_r\right] e^{-j2\pi f_r r_o/q} h\left[\frac{x_f - (x_o-x_s)/p}{L/p}\right]$$

$$\times e^{-j\pi \frac{c_a p^2}{q r_o} f_r (x_f-x_o/p)^2} e^{-j2\pi \frac{c_a p^2}{\lambda_r r_o} (x_f-x_o/p)^2} \qquad (39)$$

where $c_3 = \exp[-j4\pi r_o/\lambda_r]$ is a complex constant. The undesired exponential

in $f_r x_f^2$ is caused by range curvature. The last exponential is the desired azimuth focussing-term. From the techniques used in Appendix C it may be shown that the one-dimensional transform with respect to x_f is

$$G_x(f_x,r_f) = \sigma c_4 \, f\left\{\frac{2q}{c}\left[r_f - \frac{r_o}{q} - \frac{\lambda^2 r_o f_x^2}{8c_a p^2 q}\right]\right\}$$

$$\times h\left(\frac{f_x - \frac{2c_a p}{\lambda_r r_o} x_s}{-2c_a p\beta/\lambda_r}\right) e^{j \frac{\pi\lambda_r r_0}{2c_a p^2} f_x^2} e^{-j2\pi f_x x_o/p} \qquad (40)$$

where c_4 is a complex constant. The exponential in f_x^2 is the desired focussing term free of range-curvature aberrations. Range curvature appears as an offset in range of the function f.

5. IMAGE FORMATION

5.1 GENERALIZED PROCESSING

The object of signal processing is to take an input signal and produce an output image. For a point object at (x_o,r_o) it is required to produce a point image at $(x_2,r_2) = (M_x x_o/p, M_r r_o/q)$ where (x_2,r_2) are the azimuth and range dimensions in the output plane, M_x is the azimuth magnification and M_r is the range magnification. For unity aspect ratio we require that $M_x/p = M_r/q$. In this section it is assumed that aberrations are fully corrected so that only ideal images are discussed. A discussion of image degradations will be included in Section 7.

The image $R(x_2,r_2)$ is produced by performing the two-dimensional correlation

$$R(x_2,r_2) = \iint_{-\infty}^{\infty} g(x_f,r_f) g^*_{ref}(x_f - x_2,\ r_f - r_2)\, dx_f dr_f. \qquad (41)$$

The reference function is given by

$$g_{ref}(x_f,r_f) = w_x\left(\frac{x_f + x_s/p}{D_x/p}\right) f\left[\frac{2q}{c}\left(r_f - \frac{c_a p^2}{2qr_o} x_f^2\right)\right]$$

$$\times e^{-j \frac{2\pi c_a p^2}{\lambda_r r_o} x_f^2} \qquad (42)$$

where w_x is a window function and D_x is its width. The correlation (41) may be done directly as indicated or by matched filtering, wherein the spectrum $G(f_x,f_r)$ of (29) is multiplied by a reference spectrum

$$G^*_{ref}(f_x,f_r) = c_2\, F^*\left(\frac{cf_r}{2q}\right) W_x\left[\frac{f_x - (2c_a p/\lambda_r r_o)x_s}{pD_{fx}}\right] \times e^{\frac{-j\pi\lambda_r r_o f_x^2}{2c_a p^2}} e^{\frac{j\pi\lambda^2 r_o r_r f_r^2}{4c_a p^2 q}} . \quad (43)$$

The first exponential is a focussing function and the second corrects for range curvature. The product GG^*_{ref} is inverse transformed to produce the image $R(x_2,r_2)$.

The correlation may also be performed as a combination of direct correlation in one of the two dimensions and by matched filtering in the other. Different operations such as focussing and range-curvature correction may be performed independently and at different stages.

In the object domain, the x axis was chosen such that it is parallel to the velocity $\underline{V}/c_a$ over the surface. This velocity makes an angle $(\phi_s - \theta_{ye})$ with the local meridian as shown in Figure 1(b). The output image axis x_2 is also oriented parallel to $\underline{V}/c_a$, i.e., at an angle $(\phi_s-\theta_{ye})$ to the local meridian. Since both ϕ_s and θ_{ye} vary with latitude, the orientation of the x_2 axis varies with latitude. It is assumed that this variation is sufficiently slow that $(\phi_s - \theta_{ye})$ can be considered constant over at least a synthetic-aperture length.

5.2 OUTPUT WAVEFORM AND RESOLUTION

Even in the absence of aberrations a point object cannot be imaged to a perfect point image. In this section the waveform of the ideal image of a point object and the resulting resolution are discussed for both the range and azimuth dimension. It is assumed that the image is formed by the correlation operations described in Section 5.1 and therefore implied that all aberrations have been corrected.

5.2.1 Range

In a pulsed ranging system the slant-range resolution is

$$\rho_{rs} = cT_e/2 \quad (44)$$

where T_e is the effective pulsewidth of the received pulse. For a simple pulse, T_e is just the pulsewidth, and for a coded pulse, T_e is the width of the compressed pulse.

For a narrow pulse of width T_1, the transmitted range signal is represented by

$$f(t) = a_o \text{ rect}(t/T_1) \tag{45}$$

where

$$\text{rect}(t/T) = \begin{cases} 1, & -T/2 \leq t \leq T/2 \\ 0, & \text{elsewhere} \end{cases}$$

and a_o is a constant. The recorded range signal is

$$f\left[\frac{2q}{c}(r_f - r/q)\right] = a_o \text{ rect}\left[\frac{r_f - r/q}{R_1/(2q)}\right] \tag{46}$$

where $R_1 = cT_1$ is the pulse length in space. For practical reasons a long coded pulse is usually used. In SAR the most commonly used coded pulse is the chirp waveform. The transmitted range signal is

$$f(t) = a_o \text{ rect}(t/T_2)e^{j\pi st^2} \tag{47}$$

where T_2 is the pulsewidth and s is the sweep rate in Hz/s. The recorded range signal is

$$f\left[\frac{2q}{c}(r_f - r/q)\right] = a_o \text{ rect}\left[\frac{r_f - r/q}{R_2/(2q)}\right] e^{j\pi s(2q/c)^2(r_f - r/q)^2} \tag{48}$$

where $R_2 = cT_2$ is the pulse length in space.

If the range correlation in (41) is performed for f as given in (48) and if the width D_x of the window function w_x is large compared to L, then the envelope of the resulting compressed signal is

$$\left| c_5 a_o \text{ sinc}\left[\frac{R_2}{2q} s\left(\frac{2q}{c}\right)^2\left(\frac{r_2}{M_r} - r/q\right)\right]\right| \tag{49}$$

where sinc $x = \sin \pi x/(\pi x)$ and c_5 is a complex constant. For $D_x = L$ a more complex form results although (49) remains a good approximation, especially near the main peak at $r_2 = M_r r/q$. The dependence of r on x_f in (49) must be removed in the processing so that the sinc function is centred on $r_2 = M_r r_o/q$ as required. The range compression can be performed separately before recording the input signal, in which case the input range signal has the form of (49) where r_2/M_r is replaced by r_f.

By omitting the magnification factors, we obtain the resolution in terms of unscaled dimensions. From (49), the Rayleigh slant-range resolution is

$$\rho_{Rrs} = \frac{c}{2}\left(\frac{1}{s\, R_2/c}\right) = \frac{c}{2} T_e \tag{50}$$

where $T_e = 1/B_{vr}$ and $B_{vr} = sT_2$ is the bandwidth of the chirp signal. If a weighting is used the output is no longer a sinc function. The -3 dB width of the compressed pulse is defined as the resolution

$$\rho_{3rs} = \frac{u_r c}{2B_2} \tag{51}$$

where u_r is a weighting constant (which, for example, is 0.886 for uniform weighting and 1.33 for Hamming weighting). Because of the one-to-one correspondence between time and frequency pointed out in Appendix C, a weighting of $w_r(r_f)$ in the input plane or a weighting $w_r[c^2 f_r/(4q^2 s)]$ in the frequency plane results in approximately the same output.

The ground-range resolution ρ_{rg} is found from the slant range by differentiating (2) or (3) so that

$$\rho_{rg} \simeq \rho_{rs}\, c_r r_o / \sqrt{r_o^2 - h_s^2} \quad , \tag{52}$$

a function of range r_o.

5.2.2 Azimuth

The azimuth image is obtained by performing the azimuth correlation in (41). For g given by (28) and g_{ref} given by (42) the azimuth correlation reduces to

$$R(x_2) = \int_{-\infty}^{\infty} h\left(\frac{x_f - \frac{x_o - x_s}{p}}{L/p}\right) w_x\left(\frac{x_f + x_s/p - x_2}{D_x/p}\right) e^{-j2\pi\left(\frac{2c_a p^2 (x_2 - x_o)}{\lambda_r r_o}\right) x_f} dx_f \; e^{\frac{j2\pi c_a p^2 (x_2^2 - x_o^2)}{\lambda_r r_o}} . \tag{53}$$

The phase factor in $x_2^2 - x_o^2$ has no effect on the image intensity and is hereafter omitted. It was assumed that the range-curvature effects appearing in the range function f have been taken care of appropriately (see Section 5.3). The azimuth point-spread function (impulse response) is then the Fourier transform of the product hw_x. If, for example, both h and w_x are rect functions and $D_x >> L$, then the envelope of the azimuth point-spread function is proportional to

$$\text{sinc}\left[L\, \frac{2c_a p}{r_o \lambda_r}\left(\frac{x_2}{M_x} - x_o/p\right)\right] . \tag{54}$$

The unscaled azimuth Rayleigh resolution is $\rho_{Ra} = \lambda_r/(2c_a\beta)$ and the -3 dB resolution $\rho_{3a} = 0.886\, \lambda_r/(2c_a\beta)$. Often, a uniform antenna of width D is

considered and the Rayleigh beamwidth of $\beta = \lambda_r/D$ is taken as the beamwidth over which the beam pattern is uniform. Then, $\rho_{Ra} \simeq D/2$. In general, the -3 dB resolution is

$$\rho_{3a} = \frac{u_a \lambda_r}{2c_a \beta} \tag{55}$$

where u_a is a weighting constant that depends on the form of h and w_x. Similar results are obtained by utilizing a window $W_x(f_x/D_{fx})$ in the frequency plane.

If w_x and h are rect functions and $D_x = L$, then the envelope of the azimuth point image is proportional to

$$\left| (1-p|x_2''|/L)\ \text{sinc}\left[\frac{2c_a p}{\lambda_r}\ \beta\ (1-p|x_2''|/L)x_2''\right] \right|, \quad |x_2''| \leq L \tag{56}$$

and is 0 elsewhere. Here, $x_2'' = x_2/M_x - x_o/p$. Around the central peak at $x_2 = x_o/p$, (54) and (56) are nearly identical and therefore the resolutions are nearly identical. Although form (56) has the slight advantage of having no sidelobes for $x_2'' > L$, most successful correlators to date [1] generate outputs with the form (54).

5.3 RANGE-CURVATURE CORRECTION

In the input signal of (28), range curvature appears in the function f as a quadratically varying offset in r_f equal to $c_a p^2 (x_f - x_o/p)^2/(2qr_o)$. If direct correlation of the input were to be performed as in (41) then the reference function (42) would have to contain a function f with the same quadratic warp. Note that the quadratic is a function of r_o and therefore the reference should be changed with each new value of r_o. However, if the input signal is slowly varying with r_o, a single reference may be adequate over a certain spread of ranges (see Section 7).

In the two-dimensional frequency plane it is seen from expansion (30) that the effect of range curvature appears as the separate phase term

$$\exp\left[-j\ \frac{\pi\lambda^2 r_o f_r f_x^2}{4c_a p^2 q}\right] .$$

If this term is multiplied by a filter function whose argument is its complex conjugate then the product is unity and the effects of range curvature are cancelled. The filter function can be part of G_{ref}^* given by (43) or it can be used separately. This rather complicated filter is a two-dimensional phase function of $f_r f_x^2$ and is range dependent. Again, as discussed in Section 7, a single reference may be adequate over a certain spread of ranges.

Range-curvature correction may also be performed in either the (x_f, f_r) domain or the (f_x, r_f) domain. Leith [6] demonstrates a method of multiplying

the function $G_r(x_f,f_r)$ of (39) by a correction factor $\exp[j\pi c_a p^2 f_r(x_f-x_o/p)^2/(qr_o)]$ which is a phase function in both f_r and x_f^2. The range curvature is thereby eliminated. Unfortunately, not only is the correction dependent on range r_o, but the correction is good for only one value of x_o. In the function $G_x(f_x,r_f)$ of (40) it is seen that range curvature may be corrected by shifting the function f by an amount $-\lambda_r^2 r_o f_x^2/(8c_a p^2 q)$ in the r_f direction. The shift is dependent on both range r_o and azimuth frequency squared. However, by reasoning similar to that used in Section 7, there may be a substantial spread of ranges over which a single shift may be adequate. Note that the shifting in r_f is the equivalent to applying the linear phase shift f_r in the two-dimensional transform domain. If precompression in range is utilized, the function f in (40) becomes its compressed form and signals from different ranges are separated in the (f_x,r_f) domain. This separation means that it is possible to correct for range curvature for all ranges at once. However, the shifting required is complicated, in that every point in the (f_x,r_f) domain must be shifted by amounts that vary with both r_o and f_x.

5.4 ACCOUNTING FOR ANTENNA POINTING ERROR

Antenna pointing error refers here to the deviation of the beam centre from pointing perpendicular to ground track. This error arises from pitch, yaw, equivalent yaw, and vertical velocity. Its only effect on the input function $g(x_f,r_f)$ was noted in (28) to be a shift in azimuth x_f of the antenna pattern h by the amount $-x_s/p$. Both this offset and the width of the antenna pattern are range dependent. Despite this offset, an aberration-free image is obtained when the direct correlation (41) is performed using the reference function g_{ref} given by (42). Only the window function w_x of g_{ref} is affected by the pointing error. The only problem then is the matching of position between w_x and h. Alteration of any component of g or g_{ref} other than the windows h and w_x will usually lead to image degradation as discussed later.

In matching the window function w_x to the antenna pattern h, several approaches may be taken. One approach is to make the width D_x of w_x so large that h falls within the width D_x no matter how large the shift x_s of h may be. Then the window w_x need not be offset by the amount x_s indicated in (42). If w_x and h are rect functions, the azimuth output has the form (54). Notice that the image is properly focussed and at the correct location independent of the offset x_s. Therefore it is unnecessary to determine pitch and yaw! Use of such a wide window has the disadvantage of reduced signal-to-noise ratio.

Another approach is to make $D_x = L$. Then, if w_x and h are rect functions, the azimuth output has the form (56). However, the window w_x must be shifted by exactly the distance $-x_s$ indicated in (41) so that it will be superimposed on h. Otherwise, the image will be degraded or may not even exist. Unfortunately, exact superposition is difficult to achieve. Not only do the shift x_s and width D_x have to be precisely determined, but both vary continuously with range. A practical compromise is to choose the width D_x sufficiently wide that x_s need be known only approximately but is sufficiently narrow to reduce the noise and the number of computations.

The effect of antenna pointing error in the frequency plane is seen in (29) to be a shift of only the pattern h. This shift in f_x,

$$f_{xs}(r_o) = 2c_a p x_s(r_o)/(\lambda_r r_o) \tag{57}$$

is a function of r_o as illustrated in Figure 6(a). The range function F and the phase functions are not affected. To obtain an image by matched filtering, the product GG^*_{ref} is formed. Several approaches to matching the window W_x in (43) to the pattern h in (29) may be taken. Once more, the most practical approach appears to be to make D_{fx} sufficiently wide that x_s need only be known approximately but is kept as small as possible to reduce both noise and the number of computations.

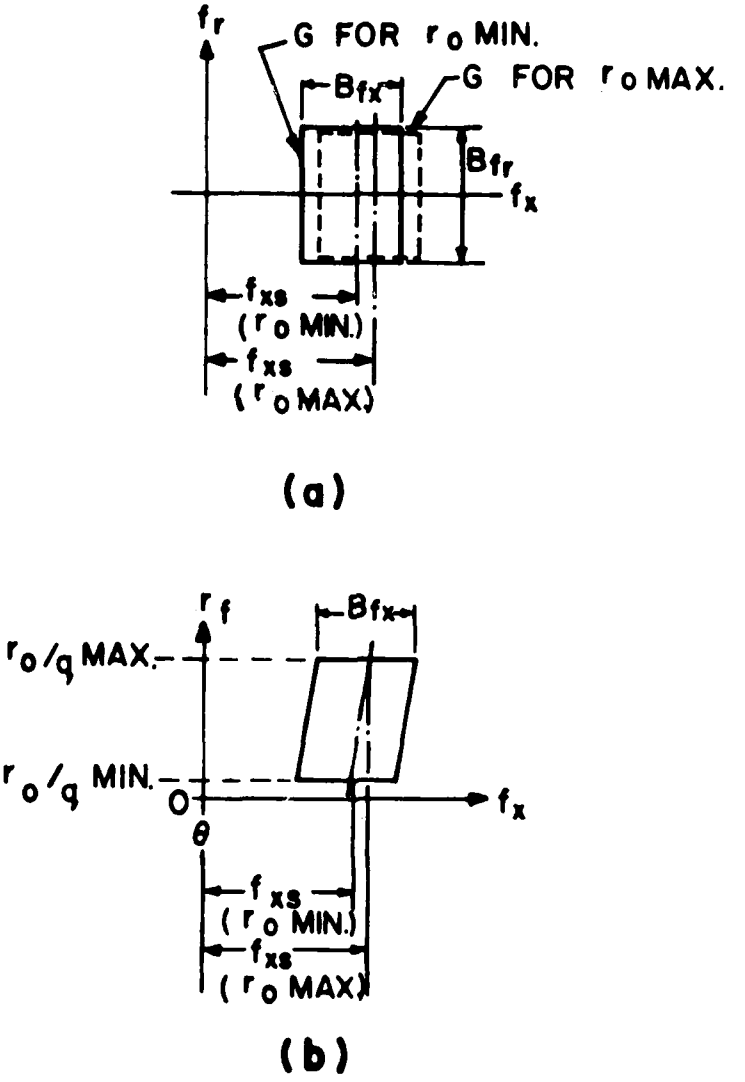

Figure 6. Outline of spectra offset by pitch and yaw for (a) two-dimensional transform and (b) one-dimensional transform

Sometimes there may be certain computational advantages in dealing with pointing error by other than the simple window shifting discussed above. One method is to "de-skew" the input (28), by tilting the lines of constant azimuth during recording so that a shift in azimuth of $x_s(r_o)$ occurs. The azimuth envelope is simplified to $h[(x_f-x_o)/(L/p)]$ but all other functions of x_f are made more complicated and the entire spectrum is offset by f_{xs} in the f_x direction. To prevent the output from being distorted, appropriate range-dependent frequency shifts could be applied or a second de-skewing used, this time on the output. Although initially attractive, this technique appears to introduce unnecessary complications.

Another method of correcting for pointing error is to do a range-dependent frequency shift of the input signal by the amount $-f_{xs}(r_o)$ so that the spectrum becomes $G(f_x + f_{xs}, f_r)$. This operation would certainly centre the azimuth envelope h in (29) on $f_x = 0$ but the phase functions of f_x would also be shifted by $-f_{xs}$. If the image were then produced by correlating against the original reference $G_{ref}(f_x,f_r)$ given by (43), the output image would be located at $x_2 = x_o - f_{xs}\lambda_r r_o/2c_a p^2) = x_o - x_s(r_o)$. This image would be distorted because of the range dependent offset. Image processing would be necessary to correct the image. Thus, frequency shifting of the input should only be used when the computational advantage gained outweighs the disadvantage of first having to perform the range-dependent shift and then having to correct for distortion (although sometimes the distortion can be tolerated).

Steering of the antenna to point perpendicular to $\underline{V}$ is highly recommended since antenna pointing error is eliminated at all ranges simultaneously. Since the signal received from an object at the instant it is abeam of the antenna has zero-doppler frequency, this steering is also called steering to the zero-doppler direction. Most airborne SAR's built to date have employed such steering with either doppler- or inertial navigation techniques to measure the pointing-angle error.

5.5 DETERMINATION OF POINTING ERROR

In Subsection 5.4 it was assumed that the shift x_s or f_{xs} caused by antenna pointing error was available to aid in image production. In this subsection, it is indicated how a value of the shift may be obtained. The accuracy required will depend on requirements for matching the window function to the antenna pattern.

The value of x_s or f_{xs} may be determined through use of separate instrumentation. The component x_{yes} can be calculated directly from orbital data. In principle the angles θ_p and θ_y could be measured by on-board detection devices such as star trackers or horizon sensors and the shifts x_{ps} and x_{ys} calculated by (23). These techniques can be very expensive and inaccurate.

A somewhat better method of determining x_s is by using the radar signal itself to find the mean frequency f_{xs} of the azimuthal spectrum (i.e., the doppler centroid). It can be seen in the spectrum $G(f_x,f_r)$ given by (29) that the amplitude variation in the f_x dimension is dependent only on h. The other terms containing f_x are phase functions only. Therefore, the mean frequency of h is also the mean frequency of $G(f_x,f_r)$ in the f_x dimension. For

simplicity we assume that the mean frequency of $h(f_x/B_{fx})$ is 0 so that the mean frequency of $h[(f_x-f_{xs})/B_{fx}]$ is just the offset f_{xs}. If the spectrum from objects at a single range can be isolated, then determination of the mean frequency automatically gives the spatial-frequency offset from which the input offset x_s can be easily determined from (57). It is only necessary to determine the total x_s and not the individual terms.

Since $x_s(r_o)$ and $f_{xs}(r_o)$ are dependent on range, it may be necessary, depending on the accuracy required, to determine their value at more than one range. Measurement could be made for each value of r_o required. Alternatively, measurement could be made at at least two values of r_o and then the remaining values interpolated.

In the estimation of f_{xs} it was assumed that the spectra for different values of r_o were separated. However, in the two-dimensional spectrum the spectra are overlapped such as illustrated in Figure 6(a). In some cases the average position of such a broadened spectrum gives a sufficiently accurate estimate of f_{xs}. If the accuracy desired requires separation in range of the spectra, a one-dimensional spectrum $G_x(f_x,r_f)$ such as illustrated in Figure 6(b) is useful. This distribution is obtained by first applying range compression to the input signal, then performing a one-dimensional transform in x_f for each constant-range line. For very accurate determination of f_{xs}, it is necessary to correct for range curvature before this stage.

In the above, the determination of f_{xs} involved calculation of the entire spectrum G. It may also be determined electronically, without the necessity of calculating the entire spectrum, by well-known techniques [11] developed for doppler navigation. For example, a simple digital version of [11] which was built in our laboratory is capable of determining f_{xs} simultaneously for 1024 different ranges, obviating the need for interpolation. Another method, which uses two narrow-band filters, has also been considered for SAR [12].

6. AMBIGUITIES

To avoid range ambiguities, the PRF, f_p, is constrained by [13]

$$f_p \leq \frac{c}{2\Delta r_s} \tag{58}$$

where Δr_s is the slant range swath width. To avoid overlap of the azimuthal spectra shown in Figure 5, the PRF is constrained by (38a) or 38b). Overlap of spectra (or "aliasing") results in azimuthal ambiguities. Restriction (38) merely states that the PRF rate must be chosen according to the sampling theorem. The effect on the output image of this overlap as f_{px} approaches and goes below the lower bound (38) has been studied experimentally [13] for azimuth offset signals. The effect of range ambiguities was also studied. In addition, the relationship of f_p and signal-to-noise ratio has been investigated for baseband digital processing [14].

Pitch and yaw aggravate the azimuth ambiguity problem by causing the envelope Σh of the repeated spectra ΣG in Figure 5 to be shifted by f_{xs}. If f_{xs} is large enough, selection of the n=0 spectrum becomes ambiguous. If the n^{th} repeated spectrum $G(f_x-nf_{xp},f_r)$ were mistakenly chosen as the n=o spectrum and correlated against the corresponding zero-order reference, $G_{ref}(f_x,f_r)$, the output for range r_o would be located in azimuth at

$$x_2 = x_o + nf_{xp}\lambda r_o/(2c_a p^2). \tag{59}$$

This equation is obtained by noting that the frequency shift nf_{xp} results in the insertion of the factor $\exp(j2\pi nf_{xp}x_f)$ in the correlation (53). The ambiguity has resulted in a range-dependent offset (distortion) of the image. There appears to be no direct method of determining from the image that a mistake in the selection of n has been made. Note that selection of the wrong spectral order could lead to incorrect correction of range curvature.

Another problem caused by the shift f_{xs} occurs when the PRF approaches the lower bound. The spectral window W_x must be accurately shifted by f_{xs} and not be wider than the bandwidth of h. Otherwise, sections of adjacent spectra will be processed along with the desired spectrum. The result is that a shifted and degraded image will be added to the desired image. Unfortunately these restrictions on window size and position preclude the techniques, described in Subsection 5.4, of using moderately wide windows to simplify the processing in the presence of antenna pointing error.

The determination of pointing error by doppler-centroid estimation techniques is made difficult as the lower bound on f_{px} given by (38) is approached. First, such things as noise, antenna sidelobes, and quantization may obscure the dip between spectra such that it is impossible to distinguish one repetition of the spectrum from the others. If pointing errors are slowly varying, time averaging of spectra may alleviate the problem. Second, the estimator could lock on to the wrong repetition of the spectrum. Third, the techniques of centroid estimation that do not require calculation of the spectrum [11], [12], may not work in the presence of high ambiguity levels. The analyses of these techniques have considered only a single spectrum to be present. Further work is required to determine if these techniques are useful as the PRF approaches the lower bound.

Ambiguity arising from pointing error may be eliminated by steering the antenna to point perpendicular to track. However, if the feedback required for pointing the antenna is obtained from a doppler-centroid estimator, then the problems discussed in the previous paragraph also arise. They will not normally be as severe because the feedback keeps f_{xs} small. Therefore, there is less chance of ambiguity, if the correct spectrum can be locked onto initially. Also, the methods not requiring spectrum analysis [11], [12] operate better when the offset is small.

7. MATCHING LIMITS

In the discussion in Section 5 on image formation it is assumed that the reference function g_{ref} was perfectly matched to the signal g or, alter-

natively, that G_{ref} was perfectly matched to G. In practice, various forms of mismatch can arise. In this section, the effects of mismatch arising from three different causes are considered. Limits to the mismatches are given.

The image degradation caused by mismatching the reference to the signal may be assessed by comparing the processor's actual point-spread function (impulse response) to the ideal correctly matched point-spread function. The degradation of the point-spread function can be a simple shift of the entire function or a dimension-dependent shift which is then called distortion. If the shape of the function is degraded it will be called here a blurring. For blurring, the quality comparison could be made on criteria such as resolution and integrated sidelobe ratio. Other image quality parameters are discussed elsewhere [15]. Such comparisons can be laborious. A simpler approach, that of using the Rayleigh quarter-wavelength rule, is utilized here.

Rayleigh took as a reference a quadratic wave converging to an ideal image of a point. It was found that, for certain aberrations, the intensity of the point image falls by less than 20% with little loss in resolution if the departure (aberration) of the actual wave from the reference wave is less than 1/4 of a wavelength. Other related criteria have been found but will not be employed here. In the present application of the Rayleigh rule, the maximum phase difference between the signal, g or G, and the reference, g_{ref} or G_{ref}, will be limited to be less than $\pi/2$ in order to maintain acceptable image quality.

The form of the phase error ϕ_e governs the type of image degradation. A phase error linear in the spatial variable merely causes a constant shift of the image. A quadratic variation corresponds to a focussing error and results in a defocussing of the image. Defocussing is one case of blurring. When ϕ_e is a function of a cross product between the two spatial variables or any of their powers, various forms of blurring of the point-spread function arise.

7.1 RANGE SPREAD

The signal g and its spectrum G are seen to be functions of target range r_o. For perfect matching it would be necessary to have a different g_{ref} or G_{ref} for every value of r_o. Sometimes continuous variation with r_o is impractical to achieve. Instead, the reference function is matched for a single range r_r. The tolerable range spread, ΔR, over which the reference and signal are adequately matched, is

$$\Delta R = r_{omax} - r_{omin}$$

$$\simeq 2(r_{omax} - r_r), \tag{60}$$

where r_{omax} and r_{omin} are the maximum and minimum values of r_o for which there is acceptable match. Often ΔR is referred to as "depth of focus". This usage is avoided here because of the possible confusion with the depth of focus that arises in optical processors for SAR signals.

The two phase factors whose matching is affected by range r_o are the azimuth-focussing factor found in either the input (28) or the transform (30), and the range-curvature factor found in the transform (30).

7.1.1 Azimuth Focussing

For azimuth focussing the phase error may be calculated for the direct correlation (41) or for the transform correlation. The range spread obtained is the same in either case. For direct correlation, a phase factor exp $j\phi_{el}$ is inserted in the azimuth correlation (53) so that the phase error is

$$\phi_{el} = \frac{2\pi c_a p^2}{\lambda_r} x_f^2 \left(\frac{1}{r_r} - \frac{1}{r_o}\right). \tag{61}$$

For notational simplicity the reference x_o is set at 0. Since ϕ_{el} is quadratic in x_f, it represents a defocussing.

In the absence of pointing errors (x_s=0), the maximum value of x_f is (L/2)/p where L is the synthetic-aperture length. By the Rayleigh rule it is required that $\phi_{el} \leq \pi/2$, so that the range spread is

$$\Delta R_1 \leq \frac{2\lambda_r r_o^2}{c_a L^2} \tag{62}$$

where $r_o^2 \simeq r_r r_o$. The substitution $r_o/L = 2c_a\rho_{Ra}/\lambda_r$ from Subsection 5.2.2 results in

$$\Delta R_1 \leq \frac{8c_a\rho_{Ra}^2}{\lambda_r} \quad . \tag{63}$$

Thus, the range spread decreases with the square of the resolution. A decrease of the wavelength increases the range spread.

In the presence of antenna pointing error, the section of the phase function utilized is centred on $x_f = -x_s$. It is now useful to substitute a new azimuth coordinate $x_f' = x_f + x_s$ into the correlation (53). Then the phase difference may be expressed as

$$\phi_{e2} = \frac{2\pi c_a p^2}{\lambda_r} [x_f'^2 - 2x_f' x_s/p + (x_s/p)^2] \frac{r_o - r_r}{r_o^2} \quad . \tag{64}$$

The component in x_s^2 is a phase constant and has no effect on the output image. Direct application of the Rayleigh rule to the first two terms of (64) results in a range spread of

$$\Delta R_2 \leq \frac{2\lambda_r r_o^2}{c_a(L^2+4Lx_s)} \tag{65}$$

which suggests that range spread can decrease considerable as x_s becomes the same order as L. However, note that the first two terms of (64) represent different aberrations. The second term inserted into the azimuth correlation integral (53) represents a linear phase shift which leads to a shift of the output point image so that it is located at

$$x_2 = x_o - x_s/p \left(\frac{r_o - r_r}{r_r}\right). \tag{66}$$

Often the image distortion (66) can be tolerated. Then the phase error ϕ_{e2} reduces to ϕ_{e1} given by (61) and the range spread ΔR_2 reduces to ΔR_1 given by (62) or (63).

7.1.2 Range Curvature

Range curvature is manifested solely as a phase function in the transform plane so that range spread is easily determined there. In the product GG^*_{ref}, the phase error resulting from mismatch is obtained from the second phase factor in (30) as

$$\phi_{e3} = \frac{\pi\lambda_r^2}{4c_a}\left(\frac{f_r}{q}\right)\left(\frac{f_x}{p}\right)^2 (r_o - r_r). \tag{67}$$

In terms of temporal frequencies given in (32) and (33),

$$\phi_{e3} = \frac{c_a \pi \lambda_r^2}{2}\left(\frac{\nu_r}{c}\right)\left(\frac{\nu_x}{V}\right)^2 (r_o - r_r). \tag{68}$$

From (35), the maximum value of ν_x is $2Vx_{max}/(r_o\lambda_r)$ where $x_{max} = L/2 + x_s$ is the maximum value of x experienced during the recording of one aperture length. The maximum value of ν_r relative to the centre of the range spectrum is $B_{\nu r}/2$ where, from (50), $B_{\nu r} = c/(2\rho_{Rrs})$. By the Rayleigh rule, the range spread is

$$\Delta R_3 \leq \frac{2\rho_{Rrs} r_o^2}{c_a (L/2 + x_s)^2} \tag{69}$$

which means that range spread deteriorates rapidly as the offset x_s approaches the beamwidth L.

It is sometimes possible to relax the limitation (69) by examining the nature of the aberration. First note that the section of the spectrum utilized is centred on $f_x = f_{xs}$, where f_{xs} is given by (57). It is then useful to replace the variable f_x in the matched filtering process by $f'_x = f_x - f_{xs}$. The phase difference becomes

$$\phi_{e4} = \frac{\pi\lambda_r^2 (r_o - r_r)}{4c_a\, qp^2}\left(f_r f'^2_x + 2f_{xs} f_r f'_x + f_{xs}^2 f_r\right) \tag{70}$$

where the maximum value of f_x' is L/2. The term in $f_{xs}^2 f_r$, being a linear phase shift, results in a shifted output image. This image distortion may often be acceptable. The term in $f_s f_r f_x'$ is sometimes inappropriately called the range walk aberration. Here it will be called the linear cross-coupling aberration. Its effect is an image blurring. A range spread may be derived for this term alone. Also it may be corrected separately. The term in $f_r f_x'^2$ is the basic range-curvature aberration alone. Its range spread is

$$\Delta R_4 \leq \frac{8\rho_{Rrs} r_o^2}{c_a L^2} = \frac{32 c_a \rho_{Rrs} \rho_{Ra}^2}{\lambda_r^2} . \tag{71}$$

which is also the range spread in the absence of pointing error (x_s=0). It is very sensitive to azimuth resolution and radar wavelength.

7.2 DEPENDENCE OF RESOLUTION ON RANGE-CURVATURE CORRECTION

Many SAR's to date have not used any range-curvature correction. Here, the limitations placed on the resolution by not performing correction are discussed, together with those arising from partial correction.

The phase error arising when no correction is used is given by (70) with r_r=0. Once again the image shift and distortion caused by the third term is not considered a serious degradation and is neglected. Only the range curvature and the linear cross-coupling blurring terms are considered. The Rayleigh rules leads to the limit

$$\left| \frac{\lambda_r^2 r_o}{16 c_a \rho_{Rrs} \rho_{Ra}^2} - \frac{\lambda_r x_s}{2 \rho_{Rrs} \rho_{Ra}} \right| \leq 1. \tag{72}$$

The first term expresses the limit of resolution on the basic range curvature and the second expresses the limit of the linear cross coupling. If the linear cross coupling is corrected separately or in the absence of pointing error (x_s=0), the limit becomes

$$\rho_{Rrs} \rho_{Ra}^2 \geq \frac{\lambda_r^2 r_o}{16 c_a} . \tag{73}$$

This result was also obtained in [6] from analysis of the input plane. (There is an arithmetic error in [6] by a factor of 4.) It shows that resolution in one dimension may be traded against resolution in the other. Reducing the wavelength greatly improves the resolution capability.

7.3 LATITUDE SPREAD

The latitude spread is the range of latitude over which the reference does not need to be altered and still give an adequate match to the signal. The altitude h_s, the earth velocity normal to track V_{en} and film recording velocity v_f can be latitude dependent.

The altitude affects the constant c_a and the slant-range-to-ground-range conversion. Normally the orbit would be chosen to hold the altitude reasonably constant over many synthetic-aperture lengths. As c_a changes, the azimuth focussing function is altered and refocussing is required as latitude changes. A latitude spread is easily derived using Rayleigh's rule. Usually the change in focus should be slight and slowly varying. The range conversion varies only slowly with latitude and should be easy to alter as necessary.

The azimuth offset x_{ye} and the ground speed V are dependent on V_{en} which in turn is dependent on latitude. The azimuth-spectrum window should be shifted appropriately as x_{ye} varies. Orbital data is all that is needed to calculate the shift. Antenna steering, as suggested previously, could be used to eliminate the shift entirely.

The velocity v_f is assumed to track ground speed V according to (20). However, it may not always be convenient to do this tracking. If v_f is constant then $p = V/(c_a v_f)$ varies with V. The most significant effect of p in the input (28) is on the azimuth focussing function. The latitude spread over which a constant focus gives acceptable imagery may be derived, again by the Rayleigh rule. Usually the spread is very large compared to a synthetic-aperture length.

8. MIXED INTEGRATION

SAR images of diffuse extended targets can have a granular appearance, sometimes called speckle, arising from the fact that the microwave illumination is coherent. Image quality may be improved either by improving resolution by means of increased coherent integration or by improving the signal-to-noise ratio by incoherent averaging of images. Resolution ρ is inversely proportional to coherent-integration length. Signal-to-noise ratio, defined as the ratio of the mean of the image intensity to it's standard deviation, is increased by a factor $\sqrt{N}$ where N is the number of independent images incoherently averaged. In SAR, the practical forms of incoherent averaging, sometimes called mixed integration [16] or multiple-look processing, are implemented at the sacrifice of resolution. It is not yet clear what combination of coherent and incoherent integration leads to the best image interpretability [17], [18]. For some processing techniques, mixed integration can have the advantage that it is easier to perform than the processing required for an improvement in resolution. In this section, we look at ways of implementing mixed-integration processing. The separate images to be smoothed by incoherent averaging may be obtained from different frequency regions of the range signal (frequency diversity) or from different target aspects in the azimuth dimension (variously named time, angular, or doppler-frequency diversity [17], [18]).

As the SAR moves in the azimuth direction, a different target "look" is obtained as each aperture length is traversed. The full synthetic aperature L with resolution $\rho_a = r_o\lambda_r/(2L)$, is divided into N sub-apertures of width D_{xs} and resolution $\rho_{sub} = r_o\lambda_r/2D_{xs}$. Then the N separate images are incoherently averaged to produce a smoothed image with degraded resolution

ρ_{sub}. The division and averaging may be done in one of three equivalent ways described below.

The first method is to window the input signal given in (28) with N windows where the n^{th} window has the form $w_{xs}\{[x_f-(x_o-x_s+nX)/p]/D_{xs}\}$, X is the window spacing, and w_{xs} is often a rect function but can have tapering if desired. This window slides inside the aperture function h which is the full antenna aperture displaced by the antenna pointing error. The N sub-apertures may be processed in series or parallel and the resulting images incoherently summed. The disadvantage of input-plane windowing is that the signals for each x_o should be processed separately although the signal from a limited number of values might be processed in parallel with little degradation of image quality.

In the second method, the frequency-plane distribution given by (29) is divided into sections in the f_x dimension by windows of the form $W_{xs}[(f_x-nF_x)/D_{fs}]$ where F_x is the window spacing and D_{fs} is the window width. If $D_{fs} = D_{xs}2c_ap/(\lambda_r r_o)$, then the frequency-plane and input-plane operations result in the same resolution. Again, the sub-apertures may be processed either in series or parallel and the resulting N images incoherently summed. Obtaining multiple looks by frequency-plane division has a significant advantage in that placement of the windows is independent of azimuth position x_o. Unfortunately, it is seen from (29) that the envelope h of the spectrum shifts along f_x because of antenna pointing errors. It will usually be desirable to make the multiple-look windows track this displacement.

The third method makes use of the equivalence of convolution in the output plane and the bandpass filtering used in the frequency plane. The convolution is performed by first forming an image with the full resolution $M_x \rho_a/p$ and then incoherently averaging the intensity over a width $NM_x\rho_a/p$, which becomes the resolution of the smoothed image. The advantage of this third method is that the summation process is relatively simple. In fact, merely observing the output from a greater distance performs a similar smoothing. The method has a disadvantage in that a full resolution image must be produced.

The offsets nX in the first method and nF_x in the second have the same effect as the offsets due to pitch and yaw. Therefore the range spreads (65) and (69) are decreased by the addition of nX to x_s and increased by the replacement of the full aperture length L by the sub-aperture length D_{xs}. In the third method, the range spread is that for the full aperture L as given in (65) and (69). It is particularly important to obey the range-spread rules for multiple-look processing. If they are not followed, each look can have a different distortion making it very difficult to overlay the "looks".

Incoherent averaging may also be performed in the range dimension if the waveform bandwidth permits. Again it may be performed in 3 ways: windowing at the input, frequency-plane division with incoherent summing of images, or convolving the output image with a window. The first method is impractical and the third requires a full resolution output. The second method appears to be quite simple to implement.

Incoherent averaging techniques may be implemented in both dimensions simultaneously [16]. If MN independent images are incoherently averaged,

where M and N are the number of independent images obtained in the range and azimuth dimensions respectively, the SNR is increased by $\sqrt{MN}$.

Continuous scanning of a window across the frequency plane is possible in optical processors. For a rect window, the SNR of the output is increased by about $\sqrt{3/2}$ (0.9 dB) [16], and by almost 2 dB for a cosine (Hanning) window. Incremental scanning of a window allowing overlap of adjacent window positions is possible with digital processing. An overlap of 50% or more gives almost as much SNR gain as does continuous scanning [19].

The microwave speckle discussed above is to be distinguished from the laser speckle that arises in optical processors because of scattering by dust or imperfections of the optical elements. Laser speckle is normally reduced by using a "tracking" processor [20] to incoherently average the output image. The use of the incoherent integration techniques discussed above for microwave speckle reduction would also result in a reduction of laser speckle. Images produced by digital processors will also have a degradation that in some ways is similar to laser speckle, but is caused by the quantization and the finite word length of the processor.

9. EFFECTS OF SPURIOUS MOTION

At least three forms of motion other than the desired along-track motion of the SAR antenna can be distinguished. First, there is motion caused by earth rotation. This velocity can be large but varies sufficiently slowly to be considered constant over at least one synthetic-aperture length. This motion was simply handled by choosing a coordinate system fixed to the surface. Second, there may be motion of individual objects, such as vehicles, relative to a fixed background. MTI techniques may be useful here [7]. Similarly, there can be motion of one section of the object fields such as in one model of ocean-wave motion [10]. Third, there are spurious motions of the SAR itself. The form of the input function in the presence of spurious motion of the object will be presented. Then the effects on the image of spurious motion of both the object and the SAR are discussed. Some comments on correction are made.

Let the point object located at point A_o (see Figure 1) have, at time $t=t_o$, a velocity $\underline{V}_o$ along the surface. It has components $\underline{V}_{op}$ parallel to the SAR velocity $\underline{V}/c_a$, $\underline{V}_{on}$ normal to $\underline{V}/c_a$, and $\underline{V}_{ov}$ vertical to the surface. The range r may then be derived by techniques followed in Section 2. If terms in x^3 and higher are neglected, then

$$r \simeq r_o + \frac{c_a V_{or}}{V}(x-x_o) + c_a\left(\frac{V_1}{V}\right)^2 \frac{(x-x_o)^2}{2r_o} \tag{74}$$

where

$$V_{or} = \frac{V_{on}\sqrt{r_o^2-h_s^2}}{c_r r_o} - \frac{h_s V_{ov}}{r_o} \tag{75}$$

is the radial velocity of the object,

$$V_1^2 = V_p^2 + \frac{r_o^2 - h_s^2}{r_o^2} V_{ov}^2 + \left(\frac{h_s}{r_o}\right)^2 (c_a V_{on})^2, \tag{76}$$

and

$$\underline{V}_p = \underline{V} - c_a \underline{V}_{op}$$

is the relative velocity between the SAR and the object in the direction of $\underline{V}$. The factor V_1^2 is just the sum of the squares of all velocity components perpendicular to the radial line. Usually the first term dominates so that $V_1^2 \simeq V_p^2$. Raney [7] derived a similar result and included object acceleration. If the squares are completed, r may be also written as

$$r \simeq r_o + \frac{c_a}{2r_o}\left(\frac{V_1}{V}\right)^2 [x - x_o + x_m(r_o)]^2 - r_m(r_o) \tag{77}$$

where

$$x_m(r_o) = \frac{V_{or} V r_o}{V_1^2} \tag{78a}$$

and

$$r_m(r_o) = \frac{c_a V_{or}^2 r_o}{2V_1^2} \tag{78b}$$

are, respectively, azimuth and range offsets caused by object motion and are both functions of r_o. A similar form describing the effect of object motion in terms of offsets has been given by Elachi and Brown [10, p. 90]. For V_o=0, both (74) and (77) reduce to (12).

In the recorded signal, the range r affects the range function $f[(2/c)(qr_f - r)]$ and the azimuth focussing function $\exp(-j4\pi r/\lambda_r)$. For both forms of r, one manifestation of the object motion in the focussing function is the weighting $(V_1/V)^2$ which results in a defocussing. Since $V_1 \simeq V_p$, the along-track velocity component is the main cause of this defocussing.

For form (74), the range function has a displacement linear in $x-x_o$ caused by the radial velocity V_{on}. Such displacement in range is sometimes referred to as "range walk". This linear term in the focussing function represents an azimuth-frequency offset. If form (77) is used, the range function and the focussing function may be described as being offset in azimuth by x_m and in range by r_m.

Image production for a moving object is made difficult because the velocity $\underline{V}_o$ is usually not known. Consider first the defocussing weighting $(V_1/V)^2$. It becomes unity as V becomes large compared to V_o. Therefore, defocussing can often be negligible. If it is not, then the processor may

be "refocussed" by trial and error until a satisfactory image has been obtained. This technique has been used to try to image ocean waves. Objects not moving at velocity $\underline{V}_o$ will be defocussed.

Consider now the offsets x_m and r_m. If the recorded signal with r given by (77) were correlated against a non-shifted reference and the focussing were suitably adjusted, then the output point image would be located at $(x_2,r_2) = [x_o - x_m(r_o),\ r_o - r_m(r_o)]$ where magnification factors have been omitted. Furthermore these offsets are valid for only one value of azimuth x_o. An object, also with a velocity $\underline{V}_o$ but located at $(x_o + \Delta x, r_o)$ where Δx is some azimuthal increment, will be imaged at

$$(x_2,r_2) = [x_o + \Delta x - x_r(r_o), r_o + (V_{or}/V)\Delta x - r_r(r_o)]. \tag{79}$$

The extra shift in range results from the fact that the object at $(x_o+\Delta x, r_o)$ moves a distance $(V_{or}/V)\Delta x$ in slant range in the time it takes the SAR to move from x_o to $x_o + \Delta x$.

If the SAR antenna has a spurious velocity $(-c_a\underline{V}_o)$ in addition to the desired velocity $\underline{V}$, then the equation for range r will again be given by (74) or (77). Thus, the effects of spurious motion of the antenna are the same as those of object motion. The trial and error methods used for dealing with object motion may be used for antenna-motion errors. However, advantage is usually taken of the fact that the value of the antenna-velocity error can be obtained. It may be obtained from orbital data for satellite-borne SAR and from inertial- or doppler-navigation systems for airborne SAR. Two classes of antenna motion are considered here.

In the first class of spurious motion, the velocity error is considered to be very slowly varying (constant over many aperture lengths). Such errors are commonly associated with satellite-borne SAR but can arise on airborne SAR because of such things as the constant error of the velocity measurement. The effects of such simple velocity errors are easily corrected by techniques already encountered. The along-track error can be corrected either by altering the recording film velocity v_f so that scale factor p is constant or by equivalently altering the scale factor during image processing. The vertical velocity component can be dealt with as an additional pitch of the antenna. The horizontal cross-track component may be dealt with in the same way as was earth rotation.

In the second class of spurious motion, the velocity error may vary even during one synthetic-aperture length but the error itself is relatively small. Such spurious motion is commonly associated with airborne SAR and arises from air turbulence. The effects of these velocity variations are best described through detailed analysis using range r given by (74) and are usually corrected by applying motion compensation directly to the received signal itself. The along-track velocity variation is compensated by varying the recorder velocity v_f and therefore the azimuth scale factor p. If frequency offset in azimuth is used, the offset frequency must also be varied so as to hold the spatial offset f_{ox} constant. Similarly, the PRF must be varied so as to hold the sample spacing constant on the recording. (If the spacing varies during an aperture length, the azimuth spectrum is broadened.) The radial-velocity error V_{or} may be seen from (74) to give rise to a

frequency shift of the azimuth focussing function. A phase shift may be applied to the radar frequency to compensate. Although V_{or} is dependent on range r_o, a single compensating frequency shift is usually used over a broad spread of ranges since the variation V_{or} is usually small.

Occasionally, there may be a radial acceleration [7] that causes a quadratic phase-error sufficiently large to defocus the signal. Often it is fairly simple to refocus by trial and error.

In the above derivation of range r, terms in x^3 and higher were neglected. Such terms arise in the Taylor expansion from spurious motions having acceleration or higher derivatives in the along-track direction or having third and higher derivatives in the radial direction. Recall that for the azimuth focussing function, a linear term causes a shift of the output image and a quadratic error causes a defocussing that often can be refocussed. However, higher-order terms cause an image blurring that are not so easily corrected. Processing is considerably simplified when these terms can be neglected. For the range function f, the linear and quadratic terms relate to range walk and range curvature respectively. The higher-order terms will not normally be large enough to cause image degradation.

10. SUMMARY

A unified description of the signal received by a SAR is presented, which accounts for the effects of flight-path curvature, surface curvature, range curvature, the earth's rotation and antenna pointing errors. Curvature of the flight path and of the earth's surface is handled taking the azimuth coordinate as lying along the curved surface. The direct effects of the earth's rotation are eliminated by aligning the azimuth coordinate with the trajectory of the orbit along the surface itself. The two-dimensional Fourier transform of the recorded signal is derived. It is found that filtering in the two-dimensional transform plane is an attractive method of correcting for range curvature although several other techniques are worth considering. The effects of antenna pointing errors due to the pitch and yaw of the vehicle, and to the equivalent yaw caused by the earth's rotation, are found to be limited to a shift in the azimuthal frequency of the spectral envelope. All that is then needed to obtain an image free of aberrations is to centre the processing window on this shifted envelope. No other modification to the processing is required. Steering the antenna to point to the zero-doppler direction eliminates this shift problem entirely.

It is shown that azimuthal focussing can be carried out using the same correlation reference function over an interval of ranges without seriously degrading the quality of the image. A corresponding range interval for range-curvature correction is derived. The range interval for azimuthal focussing is usually much smaller than for range-curvature correction. The trade-offs between resolution in range and azimuth in the presence of range curvature are derived. The resolution obtainable with no correction at all is given. Some methods of implementing incoherent integration to reduce microwave speckle are described.

Motion of the object results in an image that is offset from the correct position but is usually still in focus. Slowly varying motion errors of the SAR itself can usually be corrected for by the simple techniques used to correct for the effects of the earth's rotation and pointing errors. The effects of rapidly varying velocity errors of low amplitude can be corrected by motion-compensation techniques.

11. ACKNOWLEDGEMENT

The valuable contributions of M.R. Vant and G.E. Haslam are acknowledged with appreciation.

This work is supported by the Department of National Defence, Research and Development Branch.

12. REFERENCES

1. Cutrona, L.J., E.N. Leith, L.J. Porcello and W.E. Vivian, *On the Application of Coherent Optical Processing Techniques to Synthetic Aperture Radar*, Proc. IEEE, Vol. 54, pp. 1026-1032, August 1966.

2. Brown, W.M., *Synthetic Aperture Radar*, IEEE Trans. Aerospace and Elect. Syst., Vol. AES-3, pp. 217-229, March 1967.

3. Harger, R.O., *Synthetic Aperture Radar Systems*, New York: Academic Press, 1970.

4. Tomiyasu, K., *Tutorial Review of Synthetic-aperture Radar (SAR) With Applications to Imaging of the Ocean Surface*, Proc. IEEE, Vol. 66, pp. 563-583, May 1978.

5. Vant, M.R. and G.E. Haslam, Private Communications, Communications Research Centre, Ottawa, Ontario, Canada.

6. Leith, E.N., *Range-azimuth-coupling Aberrations in Pulse-scanned Imaging Systems*, J. Opt. Soc. Am., Vol. 63, pp. 119-126, February 1973.

7. Raney, R.K., *Synthetic Aperture Imaging Radar and Moving Targets*, IEEE Trans. Aerospace and Elect. Sys., Vol. AES-7, pp. 499-505, May 1971.

8. Tomiyasu, K., *Phase and Doppler Errors in a Spaceborne Synthetic Aperture Radar Imaging the Ocean Surface*, IEEE J. Oceanic Eng., Vol. OE-1, pp. 68-71, November 1976.

9. Crane, R.K., *Ionospheric Scintillation*, Proc. IEEE, Vol. 65, pp. 180-199, February 1977.

10. Elachi, C. and W.E. Brown, *Models of Radar Imaging of the Ocean Surface Waves*, IEEE Trans. Ant. and Prop., Vol. AP-25, pp. 84-95, January 1977.

11. Kobayashi, M., H. Osawa, N. Morinaga and T. Nawekawa, *On the Mean Frequency Measurement System using Correlation Detection*, IEEE Trans. Aerospace and Electronic Systems, Vol. AES-10, pp. 364-371, May 1974.

12. Zelenka, J.S., *Optimization of a Frequency Tracker*, Ph.D. Thesis, University of Michigan, Ann Arbor, Michigan, 1966.

13. Leith, E.N., A.A. Freisem and A.T. Funkhouser, *Optical Simulation of Radar Ambiguities*, IEEE Trans, Aerospace and Elect. Sys., Vol. AES-6, pp. 832-839, November 1970.

14. Zeoli, G.W., *A Lower Bound on the Data Rate for Synthetic Aperture Radar*, IEEE Trans. Inf. Th., Vol. IT-22, pp. 708-715, November 1976.

15. Musoff, H., G.T. Schmidt and G.L. McFarland, *Motion-compensation Requirements for a Synthetic-aperture Radar (SAR)*, NAECON '76 Record, pp. 540-547, 1976.

16. Zelenka, J.S., *Comparison of Continuous and Discrete Mixed-integrator Processors*, J. Opt. Soc. Am., Vol. 66, pp. 1295-1304, November 1976.

17. Mitchell, R.L., *Models of Extended Targets and Their Coherent Radar Images*, Proc. IEEE, Vol. 62, pp. 754-758, June 1974.

18. Porcello, L.J., N.G. Massey, R.B. Innes, and J.M. Marks, *Speckle Reduction in Synthetic-aperture Radars*, J. Opt. Soc. Am., Vol. 66, pp. 1305-1311, November 1976.

19. Welch, P.D., *The Use of Fast Fourier Transform for the Estimation of Power Spectra: A Method Based on Time Averaging Over Short, Modified Periodograms*, IEEE Trans. Audio and Electroacoustics, Vol. AU-15, pp. 70-73, June 1967.

20. Kozma, A., E.N. Leith and N.G. Massey, *Tilted-plane Optical Processor*, App. Opt., Vol. 11, pp. 1766-1777, August 1972.

21. Rihaczek, A.W., *Principles of High-Resolution Radar*, New York: McGraw-Hill, 1969, p. 227.

APPENDIX A

Derivation of V_{en} and V_{ep}

A brief description of (5a) and (5b) are given here. Refer to Figure 2. From rules of spherical trigonometry for right spherical triangles we have

$$\cos\phi_s = \tan\phi_{lat}\cot\phi_o \tag{A.1}$$

and

$$\sin\theta_i = \sin\phi_{lat}/\sin\phi_o. \tag{A.2}$$

The velocity components are

$$V_{en} = (\omega_e r_e \cos\phi_{lat})\cos\phi_s \tag{A.3}$$

and

$$V_{ep} = (\omega_e r_e \cos\phi_{lat})\sin\phi_s. \tag{A.4}$$

After some manipulation and the use of $\sin\phi_s = \sqrt{1 - \cos^2\phi_s}$, (5a) and (5b) are obtained.

APPENDIX B

Block Diagrams for Generating and Demodulating SAR Signals

A simplified block diagram is given here for each of the three methods of generating and demodulating the SAR signal. Many variations of these circuits are possible. They were chosen to illustrate the principle and not necessarily to be a recommended circuit. In all three forms shown in Figure B1, the stable local oscillator (stalo) generates a signal of frequency f_c that is used both as the radar carrier and for demodulating the return signal. As a result, the stalo frequency is accurately eliminated from the output signal. All the boxes marked "mixer" include an appropriate low-pass filter. For azimuth offset, the offset frequency f_o is much less than f_c. Thus, f_o need not be extremely stable. For range offset, frequency dividers and multipliers are used to maintain the proper relationship between f_o and f_p. For baseband operation, a 90° phase shifter is used. In-phase (I) and quadrature (Q) components are produced.

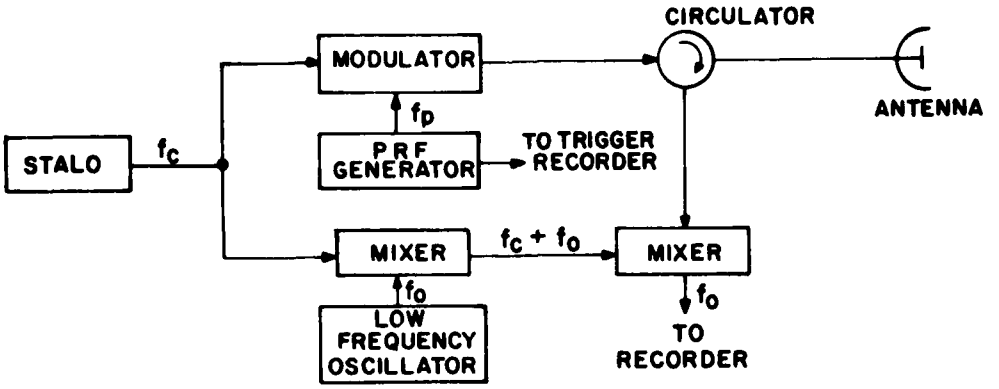

(a) AZIMUTH OFFSET

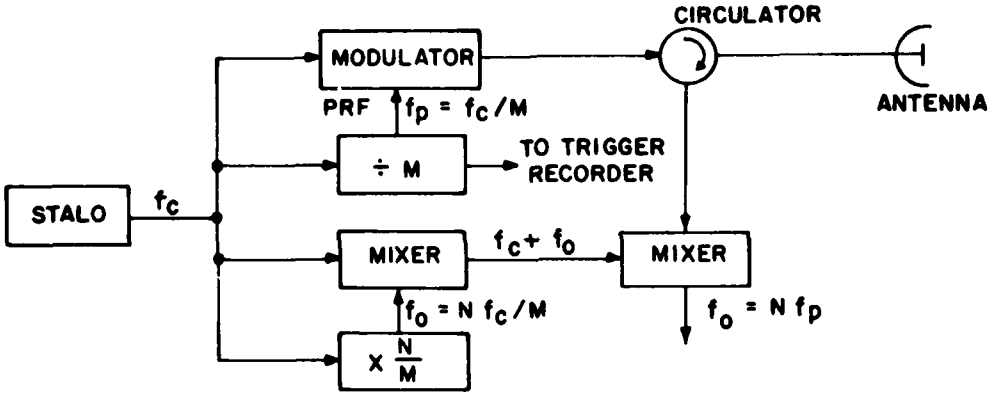

(b) RANGE OFFSET

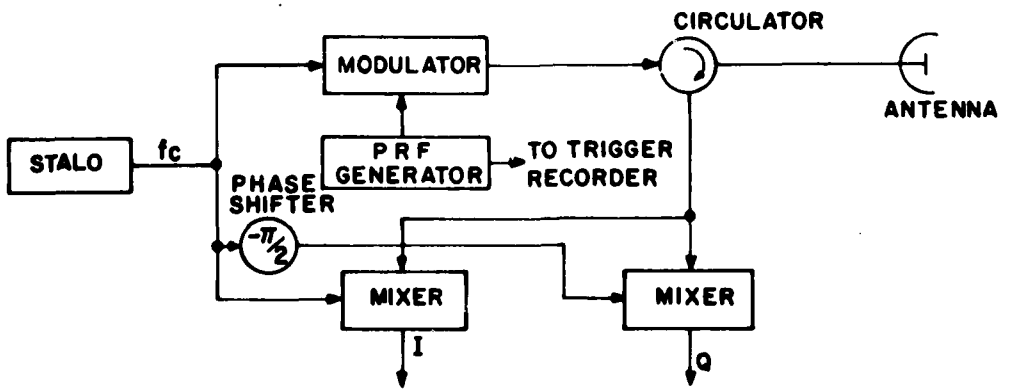

(c) BASEBAND OPERATION

Figure B1. Simplified circuits for generating input to recorder for (a) azimuth offset, (b) range offset and (c) baseband operation

APPENDIX C

Derivation of the Fourier Transform

In this Appendix, (29) is derived. First, perform the Fourier transform with respect to r_f of the function $g(x_f,r_f)$ given by (28). If the function in f_o and the c.c. terms are omitted, the following is obtained:

$$G(f_x,f_r) = \sigma F\left(\frac{c}{2q} f_r\right) e^{-j2\pi f_r r_o/q} e^{-j\frac{4\pi}{\lambda_r r_o}}$$

$$\times \int_{-\infty}^{\infty} h\left(x_f - \frac{x_o - x_{py}(r_o) - x_{ye}(r_o)}{\frac{p}{L/p}}\right) e^{-j\pi[f_r + 2q/\lambda_r]\frac{c_a p^2}{qr_o}(x_f - x_o/p)^2} e^{-j2\pi f_x x_f} dx_f. \tag{C.1}$$

Consider a linear FM waveform $h(t)\exp[j\pi kt^2]$ where $h(t)$ is a real envelope and k is the sweep rate in Hz/sec. If the time-bandwidth product is large, then the spectrum $M(f)$ is given approximately by [21]

$$M(f) \simeq \frac{1}{\sqrt{|k|}} e^{j\pi/4} h\left(\frac{f}{k}\right) e^{-j\pi f^2/k}. \tag{C.2}$$

In other words, if the sweep rate is sufficiently low, there is a one-to-one correspondence between t and f.

The azimuth linear FM in (C.1) usually has a reasonably large time-bandwidth product so that rule (C.2) may be utilized. The integration over x_f is performed to obtain (29). The constant

$$1/\sqrt{|k|} = 1\Big/\sqrt{\frac{p^2 c_a}{qr_o}\left[f_r + \frac{2q}{\lambda_r}\right]}$$

is a slowly varying function of f_r near $f_r = 0$ and therefore $1/\sqrt{|k|} \simeq \sqrt{r_o\lambda_r/(2c_a p^2)}$. The antenna pattern at the transform plane is therefore

$$h\left[\frac{f_x - (f_r + 2q/\lambda_r)[pc_a x_s/(qr_o)]}{-pc_a L(f_r + 2q/\lambda_r)/(qr_o)}\right]. \qquad (C.3)$$

The terms in f_r represent the effect of range curvature on the antenna pattern. Because the function h is broad and slowly varying and because, as seen in Section 4, for most practical cases $f_r << 2q/\lambda_r$, little error in the output image is caused by neglecting f_r. Hence, the frequency plane form of h given in (29) is used.